PERGAMON

Available online at www.sciencedirect.com

SCIENCE DIRECT®

Polyhedron 22 (2003) 1921–1927

POLYHEDRON

www.elsevier.com/locate/poly

Binary metal(II)–pyromellitate coordination polymers, $M_2(pm)$ (M = Co, Fe, Mn): synthesis, structures and magnetic properties

Hitoshi Kumagai [a,b], Karena W. Chapman [c], Cameron J. Kepert [c], Mohamedally Kurmoo [a,*]

[a] Institut de Physique et Chimie des Matériaux de Strasbourg, 23 rue du Loess, 67034 Strasbourg Cedex, France
[b] Applied Molecular Science, Institute for Molecular Science (IMS), Nishigounaka 38, Myoudaiji, Okazaki 444-8585, Japan
[c] Centre for Heavy Metals Research, School of Chemistry, University of Sydney, Sydney, NSW 2006, Australia

Received 6 October 2002; accepted 13 December 2002

Abstract

The hydrothermal synthesis, structures and magnetic properties of the isostructural coordination polymers $_\infty{}^3[M^{II}_2(pm)]$, M = Co, Fe or Mn and pm = pyromellitate, 1,2,4,5-benzenetetracarboxylate, are described. The structure consists of 1D chains of edge-sharing MO_6 octahedra that are connected into layers via O–C–O bridges. The layers are held together by the pyromellitate (pm^{4-}) backbone to give a 3D structure where each ligand participates in an unprecedented 12 coordination M–O bonds to ten metal atoms. The Fe and Mn analogues are antiferromagnets whereas the Co compound displays a more complex behaviour, existing in one of three magnetic ground states at low temperature (collinear antiferromagnetism, canted antiferromagnetism and field induced ferromagnetism).

Keywords: Carboxylate; Cobalt; Iron; Magnetism; Manganese; Pyromellitate; Framework

1. Introduction

Metal-organic hybrid materials containing open-shell transition metals and connecting polycarboxylates are attracting much interest for their structural and magnetic properties [1,2]. On the one hand, the potential application of these materials in selective separations and catalysis is due to porosity that can be tuned by variation of the chemical functionality and of the dimensions and topology of the coordination network. [3]. On the other hand, the various structural motifs observed for a range of compounds provide good examples for various theoretical magnetic models of low dimensionality to be verified; in particular, one can obtain information on the balance between through-bonds and through-space exchange interactions. In addition, the metal-organic hybrids present the unique possibility to combine the properties associated with the individual components in one hybrid compound, e.g., the presence of through-space magnetic exchange may permit one to combine magnetism with porosity [4]. In view of the latter combination, our recent search for long-range magnetic ordering in low-dimensional transition metal complexes has focused on metal–carboxylate hybrid materials. In previous studies, we have characterised compounds with aromatic polycarboxylates (BDC = 1,4-benzenedicarboxylate [5] and BTC = 1,3,5-benzenetricarboxylate [6]) and saturated polycarboxylates (CHDC = 1,4-cyclohexane-dicarboxylate and CHTC = 1,3,5-cyclohexane-tricarboxylate [7]). We present a study of three transition metals pyromellitate (pm = 1,2,4,5-benzenetetracarboxylate) salts with the tetracarboxylate as the structural building block. The structure and magnetic properties of the Co(II)-pyromellitate has been reported recently [8] and here we compare its structural and magnetic properties to those of the isostructural Mn and Fe compounds.

As is common for most carboxylates, pyromellitate provides several possible coordination modes, viz: uni-

* Corresponding author. Tel.: +33-388-1071-33; fax: +33-388-107247.
E-mail address: kurmoo@ipcms.u-strasbg.fr (M. Kurmoo).

0277-5387/03/$ - see front matter © 2003 Elsevier Science Ltd. All rights reserved.
doi:10.1016/S0277-5387(03)00177-3

dentate, bis-unidentate, bidentate and tridentate, of the independent carboxylate groups. Its known multitopicity, that is the number of coordinate bonds to the number of metals, can vary from 2 to 10 coordination bonds and it can coordinate to up to ten metals as in the case of Ca and Ag or six in the Zn salt [9]. In the present study we found one example that extend these limits; it has an unprecedented 12 bonds to ten metals (Fig. 1).

2. Experimental

2.1. Synthesis

All chemicals were obtained from Aldrich and Fluka and used without further purification.

2.2. Preparation of $M_2(pm)$

$Co(OH)_2$ (0.12 g, 1.3 mmol) was suspended in distilled water ($\approx$30 ml) and a solution of H_4pm (0.25 g, 1.3 mmol) in distilled water ($\approx$30 ml) was added. The mixture was placed in the Teflon liner of an autoclave, sealed and heated to 170 °C for 6 days. It was then quenched in a water bath and allowed to cool to room temperature for 2–3 h. Violet crystals were obtained which were filtered off and washed with water and acetone and dried in air. Yield 60%. This compound was also obtained from $CoCl_2 \cdot 6H_2O$ and $Co(NO_3)_2 \cdot 6H_2O$ as starting materials.

IR bands for $Co_2(pm)$: 447m, 470m, 553s, 620s, 637s, 772s, 805s, 842m, 862m, 940m, 1136w, 1163w, 1272sh, 1305m, 1360vs, 1402ssh, 1487s, 1572sbr, 1880w.

Similar procedures using $FeSO_4 \cdot 7H_2O$ or $MnCl_4 \cdot 4H_2O$ as starting materials in similar molar ratios and at a temperature of 200 °C resulted in dichroic (brown and yellow) plate crystals of $Fe_2(pm)$ and transparent white microcrystals of $Mn_2(pm)$, respectively. These compounds were also obtained by digesting the pure metals in a boiling aqueous solution of pyromellitic acid under nitrogen. The resulting solutions were filtered hot and placed in the pressure bombs at 200 °C for 16 h.

Satisfactory chemical analyses were obtained for all three compounds.

IR bands for $Fe_2(pm)$: 440m, 460m, 550m, 614m, 636m, 770s, 804s, 838w, 862m, 938m, 1132w, 1300sh, 1360vs, 1390ssh, 1490s, 1567sbr.

IR bands for $Mn_2(pm)$: 543m, 606m, 636m, 768s, 803s, 838w, 860m, 938m, 1132w, 1298sh, 1362vs, 1399ssh, 1488s, 1570sbr.

2.3. General characterization

X-ray powder diffraction data were recorded at room temperature on two Siemens D-500 diffractometers, one equipped with monochromatized Co Kα1 ($\lambda = 1.789$ Å) and the other with Cu Kα1 ($\lambda = 1.541$ Å) radiation. Infrared spectra were recorded on a MATTSON FTIR by transmission through fine particles, prepared by crushing selected crystals, deposited on a KBr plate.

2.4. Magnetic measurements

Magnetic data were collected on a Quantum Design MPMS-XL SQUID magnetometer in the temperature range 2–300 K with fields up to 5 T. Isothermal magnetization after zero-field cooling was measured by use of a Princeton Applied Research Vibrating Sample magnetometer model 155, equipped with a continuous flow cryostat and an ITC4 temperature controller. Heat capacity was measured on pressed pellets of the compounds ($\approx$200 mg) wrapped in aluminium foil in the range 1.6–38 K. Data were taken by employing a pseudo adiabatic technique and corrected for the sample holder. ^{57}Fe-Mössbauer spectra were recorded by transmission in a bath cryostat at 77 and 4.2 K.

2.5. X-ray crystallography and structure solution

The crystals of $M_2(pm)$, M = Co or Fe, were mounted in a thin film of perfluorpolyether oil on mohair fibers. Data were collected at 150(2) K on a Bruker SMART 1000 CCD diffractometer equipped with graphite-monochromated Mo Kα radiation ($\lambda = 0.7017$ Å).

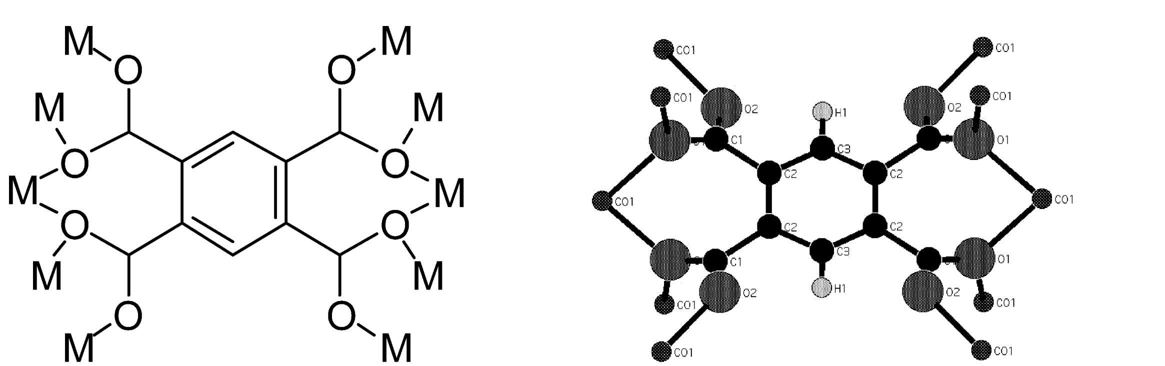

Fig. 1. Schematic representation (left) and the observed coordination mode (right) of the pyromellitate ion showing 12 coordination bonds to ten metal atoms.

Diffraction data analysis and reduction for Co_2(pm) were performed within SMART and SAINTPLUS. The data set of the Fe_2(pm) crystal showed non-merohedral twinning with two crystal domains of similar intensities rotated by approximately 180°. Indexing was achieved using GEMINI, and the individually integrated and reduced twin components were combined within GEMINI for refinement. Systematic errors in the spot integration caused by the twinning restrict the quality of this data set. The structures were solved by direct methods and expanded using Fourier techniques within SHELX-97 [10]. All non-hydrogen atoms were refined anisotropically with the carboxylate carbon in Fe_2(pm) restained to be approximately isotropic. No extinction corrections were applied. Full-matrix least-squares refinement on F_{obs}^2 converged to $R = \Sigma||F_o| - |F_c||/\Sigma|F_o|$, $R_w = [\Sigma w(|F_o| - |F_c|)^2/\Sigma w|F_o|^2]^{1/2}$ with $R_1 = 0.0292$ and $wR_2 = 0.0714$; and $R_1 = 0.0572$, $wR_2 = 0.1597$ for ($I > 2\sigma$) Co and Fe phases, respectively.

3. Results

3.1. Structure of M_2(pm)

Co_2(pm) crystallizes in the monoclinic system, $C2/m$, $a = 6.1269(12)$, $b = 17.476(3)$, $c = 4.5541(9)$ Å, $\beta = 115.531(3)°$, $V = 440.0(2)$ Å^3, $Z = 4$. The asymmetric unit of Co_2(pm) consists of one Co(II) and one quarter of the pyromellitate ligand, the latter having $2/m$ symmetry. The repeating structural motif is a uniform, zig-zag 1D chain along the a-axis consisting of edge-sharing, equivalent Co(II) ions that are bridged by oxygen atoms of pyromellitate (Fig. 2). Of the six separate pyromellitate carboxylate groups bound to each Co atom, four are involved in M–O–M bridges within the 1D chains and all six are involved in M–O–C–O–M bridges between neighbouring 1D chains. The latter, three-atom connectivity generates layers that are parallel to the ac-plane. The structure is formed of 1D zigzag chains of these edge-sharing chains of octahedral cobaltous, parallel to the a-axis. The benzene rings of the pyromellitate units connect the layers into a 3D framework through six-atom M–O–C_4–O–M bridges. The Co(II) ion has three independent Co–O bond lengths (2.029, 2.077 and 2.195 Å). The octahedra are not only distorted with regards to the distance of the oxygen atoms but also in bond angles. This distortion is characterized by bond angles of O(1)–Co(1)–O(2′), O(1″)–Co(1)–O(2‴) (159.0(1)°) and O(1′)–Co(1)–O(1″) (170.6(1)°). The 3D structure is reinforced by the presence of the strong Co–O coordination bonds with the pyromellitate units. The pyromellitate in the present case is completely deprotonated and thus carries four charges, as already found in its chemistry with transition metals that consists of various stable charges, geometries and modes of coordination. Each carboxylate unit is bonded to three cobalt atoms, as found in two other cases [5,7]. The pyromellitate ion is bonded to 10 cobalt atoms through twelve coordination bonds.

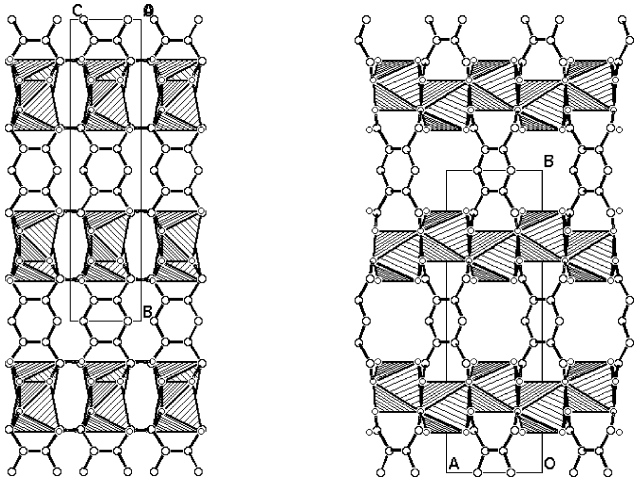

Fig. 2. View of the structure of Co_2(pm) along the (a) a-axis and (b) c-axis showing the connection between chains and layers.

Co_2(pm) exhibits a pseudo triangular topology of the magnetic ions within a layer. The nearest distance between Co atoms are 3.368 Å between those in a chain and connected via an oxygen atom, 4.475 and 4.554 Å for those between chains and connected via O–C–O bridges. The distance between the layers is 8.788 Å and the connection is via the pyromellitate backbone.

The single crystal structure determination of Fe_2(pm) showed it to be isostructural to the Co compound with $a = 6.1913(17)$, $b = 17.544(5)$, $c = 4.6009(13)$ Å, $\beta = 115.61(2)°$, $V = 450.7(2)$ Å^3. Mn_2(pm) is inferred to have a similar structure from the powder diffraction pattern, though the severe fluorescence background prevented a full Rietveld analysis to be carried out. The expanded cell dimensions of Fe_2(pm) relative to Co_2(pm) reflects the increased M–O bond lengths (2.053(3), 2.123(3) and 2.223(3) Å) consistent with the larger Fe(II) ion. The octahedral distortion apparent in the Co phase is exaggerated with characteristic bond angles of 158.24(12)° and 170.69(17)°. The tilting of the edge-sharing MO_6 octahedra forming the 1D chains is more pronounced in the Fe phase with angles of 94.25°(85.75°) compared to 93.89°(86.11°) in the Co phase.

3.2. Magnetic properties

The temperature dependence of the magnetic susceptibilities of the compounds is shown in Fig. 3. Analyses of the high temperature data are given in Table 1. The Curie constants of all three compounds lie within the limits for known divalent paramagnetic complexes [11]. The behaviour of the cobalt analogue is quite different

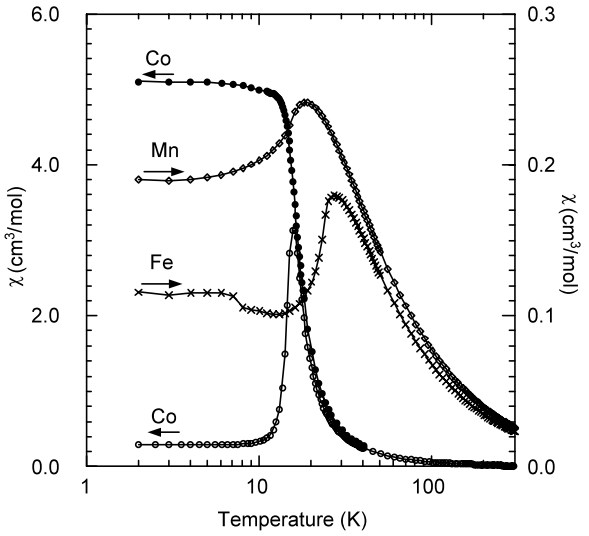

Fig. 3. Temperature dependence of the magnetic susceptibility in 100 Oe for Co_2(pm) (open circles), Fe_2(pm) (crosses), Mn_2(pm) (diamonds) and in 3000 Oe for Co_2(pm) (filled circles).

from those of the other two compounds. The dominant exchange interaction for Co_2(pm) is ferromagnetic while it is antiferromagnetic for Fe_2(pm) and Mn_2(pm). All three compounds exhibit long range antiferromagnetic ordering (Table 1) at low temperatures.

The magnetization measured in an applied field of 1 Oe and 10 kOe for Fe_2(pm) and Mn_2(pm) is similar to that measured in 100 Oe. However, for Co_2(pm) the zero-field-cool (ZFC) and field-cool (FC) magnetization in 1 Oe reveals a different behaviour and history dependence. Above 13 K the magnetization is reversible and behaves similarly to that in 100 Oe. Below 13 K there is non-reversibility and bifurcation, consistent with a weak spontaneous magnetization below the Néel transition (16 K). The weak magnetization appears to be saturated in this low field of 1 Oe and from the saturation value in 1 Oe at 2 K we estimate the canting angle to be 0.002°. For applied fields exceeding 1500 Oe, the magnetization increases below 13 K while it remains reversible above this temperature (Fig. 3). This suggests that the moments of the sublattices rotate proportionally to the strength of the applied field up to about 3000 Oe, where it starts to saturate to a value approaching the expected moment per cobalt(II).

The a.c.-magnetization for Fe_2(pm) and Mn_2(pm) measured in 1 Oe and 20 Hz is similar to the d.c.-magnetization in 100 Oe. However, that for Co_2(pm) is more complex. The in-phase component of the susceptibility (χ') exhibits a maximum at 16 K and a weak shoulder at approximately 12 K. The out of phase component (χ'') exhibits only one peak at 12 K. Measurements performed in zero d.c. bias field and an a.c. field of amplitude of 1 Oe oscillating at different frequencies (1–1000 Hz) show no frequency dependence, confirming the absence of any glassiness of the moments (Fig. 4).

The isothermal magnetization was measured at several temperatures and field ranges, employing different experimental protocols. Data taken after ZFC are shown in Fig. 5. Above 25 K the magnetization is almost linear and for $16 < T < 25$ K superparamagnetism is observed due to short-range correlation. Between T_N and $T_{canting}$ ($12 < T < 16$ K) a characteristic reversible metamagnetic behaviour is observed with a critical field increasing as the temperature is lowered. Below $T_{canting}$, hysteresis sets in and its width widens as the temperature is lowered (Fig. 5); two different loops are observed, one around zero-field and the other around the critical metamagnetic field [12]. The phase diagram, characterized by the temperature dependence of the critical field after zero-field-cooling, is shown in Fig. 6. Its form, characteristic of most metamagnets, [12] is the same as those we have observed for $Co_2(OH)_2L$, where L is terephthalate, carboxycinnamate, 4,4′-biphenyldicarboxylate, [5] but are noticeably different from those reported by others for related materials [13]. We believe that these dissimilarities may reflect different experimental protocols, in our case involving no prior magnetization of the sample in a high field, rather than fundamentally different behaviours. In the absence of hysteresis, the phase diagram derived from ZFC and FC critical fields would have been similar. The magnetization data for Fe_2(pm) and Mn_2(pm), in contrast, do not show such a rich behaviour and are as expected for classical antiferromagnets.

3.3. Heat capacity

The heat capacities (C_p) of the compounds are shown in Fig. 7. They all exhibit a sharp lambda peak consistent with the long range antiferromagnetic ordering. The sharp peaks suggest these compounds have either a 2D- or 3D-magnetic dimensionality. The

Table 1
Summary of magnetic data for M_2(pm)

M	Electronic configuration	Curie constant ($cm^3\ mol^{-1}$)	Effective moment (μ_B)	Weiss constant (K)	Néel temperature (K)
Co	d^7	5.99	4.90	+16.4	16
Fe	d^6	7.31	5.41	−9.0	26
Mn	d^5	8.00	5.66	−2.8	18

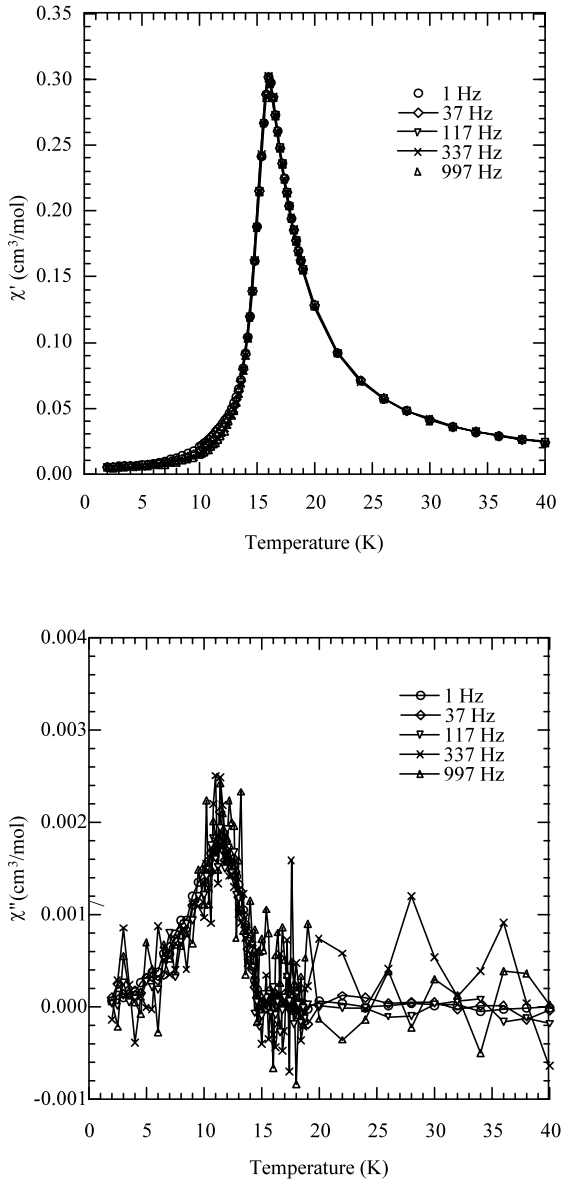

Fig. 4. Temperature dependence of the real (a) and imaginary (b) a.c.-susceptibilities for Co_2(pm).

calculated magnetic entropies ($2R\ln(2s+1)$) derived by integration of the C_p/T versus T plot up to 40 K are consistent with an $s = 1/2$ for M = Co, $s = 2$ for M = Fe, and $s = 5/2$ for M = Mn. An important point regarding the dimensionality of these compounds is that only 50–60% of the entropy is acquired up to the transition temperature. This is consistent with a 2D- rather than a one 1D- or 3D-magnetic system.

3.4. Mössbauer spectroscopy

The spectra of a polycrystalline sample of Fe_2(pm) at 77 and 4.2 K are shown in Fig. 8. In the paramagnetic region, the material displays two doublets (92 and 8%) centred at isomer shifts of 1.21 and 0.39 mm s^{-1} as

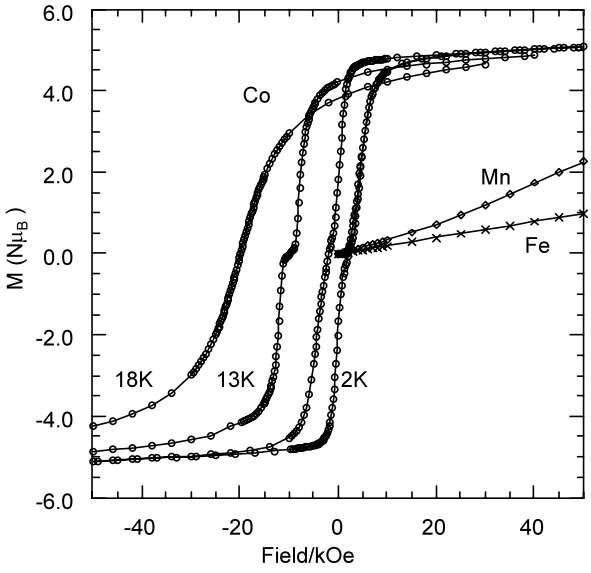

Fig. 5. Isothermal magnetization of Co_2(pm) (circles) at 18, 13 and 2 K, Fe_2(pm) (diamonds) at 2 K and Mn_2(pm) (crosses) at 2 K. The data at 18 and 13 K are offset by 20 and 10 kOe, respectively.

expected for high spin octahedral Fe^{2+} [14]. The quadrupole coupling constant is 1.44 and 1.37 mm s^{-1}, respectively. On cooling to the ordered antiferromagnetic state, the strong doublet splits into an unusual four lines of similar width centred at 0.8 mm s^{-1} with the quadrupole splitting of the outer pair being 4.85 mm s^{-1}. We estimate an internal field of 16 T at 4.2 K.

4. Discussion

The most striking structural feature of the compounds is the large number of coordination bonds the pyro-

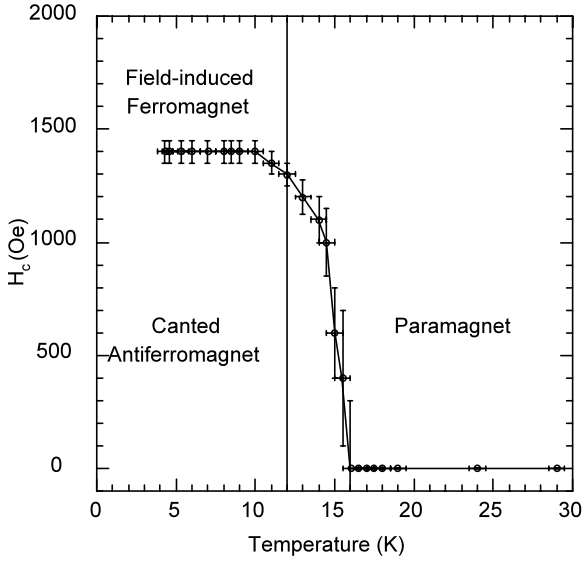

Fig. 6. Phase diagram for Co_2(pm) showing the different ground states.

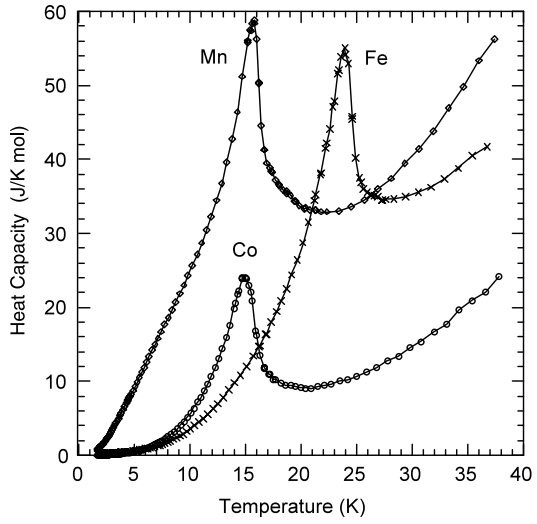

Fig. 7. Heat capacity of M_2(pm).

mellitate ligand makes with the metal ions. As such, the pm ligand may be considered as a good metal scavenger and indeed it is used for eluting metal ions in chromatography [15]. Although there appears to be some small voids visually, calculation shows no void space with contacts larger than 1.2 Å [16]. From a magnetic viewpoint, the structure may be considered as consisting of edge-shared 1D chains of MO_6 units that lie parallel to the *a*-axis, as are evident in Fig. 2(b). These chains are linked together by carboxylate bridging in the *c*-direction through all six vertices of the octahedra (Fig. 2(a)) to give a layer in the *ac*-plane. The layers are linked together through the benzene backbone of the pm ligand to give a 3D framework structure.

The difference in magnetic properties of the three compounds as well as the unusual magnetic behaviour

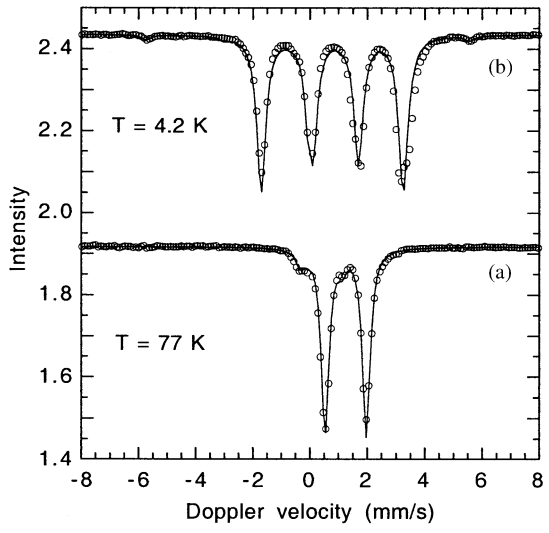

Fig. 8. Mössbauer spectra of Fe_2(pm) in the (a) paramagnetic region at 77 K and (b) ordered antiferromagnetic region at 4.2 K. The lines are fits to the data.

of Co_2(pm) (collinear antiferromagnetism, canted antiferromagnetism and field-induced ferromagnetism) deserves some comment. To rationalize these observations we can use the Goodenough and Kanamori rules for the superexchange mechanism as a starting point [17]. Three magnetic exchange pathways can be defined for this structure. The first, and possibly the strongest, is the exchange between neighbouring atoms in the chains (3.37 Å apart) and are connected by two single bridges consisting of an oxygen atom each. The M–O–M angle of 104° can give rise to either ferromagnetic or antiferromagnetic interactions depending on the electronic configurations of the metal atoms. From the observed signs of the Weiss constant, we assign this exchange to be ferromagnetic for Co_2(pm) and antiferromagnetic for Fe_2(pm) and Mn_2(pm). The second in the hierarchy is the exchange between the chains via the O–C–O bridges at distance 4.48 Å for M–O–C–O–M. From previous observations in other known compounds [8,18] we know that this exchange is weak and possibly antiferromagnetic in character. The last is that between the layers that involved the benzene backbone. The distance is 8.8 Å and the path is via O–C_4–O bridges. This interaction is therefore weaker than the second one. Anti-parallel alignment of ferromagnetic (Co) and antiferromagnetic (Fe and Mn) layers would account for the collinear long range antiferromagnetic ordering. The present observations together with those for the series $Co_2(OH)_2$(dicarboxylate) (where the dicarboxylate is terephthalate, naphthalenedicarboxylate, carboxycinnamate, or biphenyldicarboxylate in increasing length) tend to support this conclusion. For the hydroxide compounds, [5] the Néel temperature is weakly dependent on the interlayer distance while the critical metamagnetic field is very dependent. An interpretation of this observation is that the Néel temperature is independent due to the similarity of the layers, where only one exchange pathway is defined by Co–O–Co in the different compounds while the critical field scales with the interlayer exchange interactions. In the present case, the exchange interactions within the layers are slightly weakened due to the presence of two different pathways, Co–O–Co and Co–O–C–O–Co, which results in a lowering of T_N to 16 K compared to approximately 40 K for the Co–OH layered compounds.

In conclusion, pyromellitate is found to be an excellent ligand to bring together many metal atoms and for propagating efficient magnetic exchange interactions. The three compounds provide a rich variety of magnetic properties where those of the Fe and Mn compounds are easily understood but those of Co remains to be unravelled properly. Neutron diffraction and theoretical studies are needed to understand the phase diagram and the various magnetic ground states.

5. Supplementary material

Crystallographic data for the structural analysis of Co_2(pm) and Fe_2(pm) have been deposited with the Cambridge Crystallographic Data Centre, CCDC Nos. CCDC 177567 and 198710, respectively. Copies of this information may be obtained free of charge from The Director, CCDC, 12 Union Road, Cambridge, CB2 1EZ, UK (fax: +44-1223-336033; e-mail: deposit@ccdc.cam.ac.uk or www: http://www.ccdc.cam.ac.uk).

Acknowledgements

This work was funded by CNRS-France, Australian Research Council, JSPS-Japan and Royal Society of Chemistry-UK. We thank K. Heckman, C. Leuvrey and J-P. Lambour for technical assistance.

References

[1] (a) M. O'Keeffe, M. Eddaoudi, H. Li, T. Reineke, O.M. Yaghi, J. Solid State Chem. 152 (2000) 3;
(b) C.J. Kepert, D. Hesek, P.D. Beer, M.J. Rosseinsky, Angew. Chem., Int. Ed. 37 (1998) 3158;
(c) P.M. Forster, A.K. Cheetham, Angew. Chem., Int. Ed. 41 (2002) 457;
(d) A.K. Cheetham, G. Ferey, T. Loiseau, Angew. Chem., Int. Ed. 38 (1999) 3268.

[2] (a) P. Day, A.E. Underhill (eds.), Metal-Organic and Organic Molecular Magnets, Phil. Trans. R. Soc., 357 (1999);
(b) O. Kahn, Acc. Chem. Res. 33 (2000) 647.

[3] M. Eddaoudi, J. Kim, N. Rosi, D. Vodak, J. Wachter, M. O'Keeffe, O.M. Yaghi, Science 295 (2002) 469.

[4] A. Rujiwatra, C.J. Kepert, J.B. Claridge, M.J. Rosseinsky, H. Kumagai, M. Kurmoo, J. Am. Chem. Soc. 123 (2001) 10584.

[5] (a) M. Kurmoo, Phil. Trans. R. Soc. A 357 (1999) 3041;
(b) M. Kurmoo, H. Kumagai, M.A. Green, B.W. Lovett, S.J. Blundell, A. Ardavan, J. Singleton, J. Solid State Chem. 159 (2001) 343;
(c) M. Kurmoo, H. Kumagai, Mol. Cryst. Liq. Cryst. 376 (2002) 555.

[6] C.J. Kepert, T.J. Prior, M.J. Rosseinsky, J. Am. Chem. Soc. 122 (2000) 5158.

[7] H. Kumagai, M. Akita-Tanaka, K. Inoue, M. Kurmoo, J. Mater. Chem. 11 (2001) 2146.

[8] (a) H. Kumagai, C.J. Kepert, M. Kurmoo, Inorg. Chem. 41 (2002) 3410;
(b) N. Snejko, E. Gutierrez-Puebla, J.L. Martinez, M.A. Monge, C. Ruiz-Valero, Chem. Mater. 14 (2002) 1879.

[9] (a) C. Robl, Z. Naturforsch., Teil. B 43 (1988) 993;
(b) F. Jaber, F. Charbonnier, R. Faure, J. Chem. Cryst. 27 (1997) 397;
(c) C. Robl, Mater. Res. Bull. 27 (1992) 99;
(d) C. Robl, Z. Anorg. Allg. Chem. 554 (1987) 79.

[10] (a) G.M. Sheldrick, SHELXS-86 and SHELXL-93, Programs for the solution and refinement of crystal structures, University Gottingen, 1986 and 1993;
(b) M.C. Burla, M. Camalli, G. Cascarano, C. Giacovazzo, G. Polidori, R. Spagna, D. Viterbo, J. Appl. Cryst. 22 (1989) 389.

[11] A. Herpin Theorie du Magnetisme, Presse Universitaire de France, 1968.

[12] (a) P. Day, Acc. Chem. Res. 211 (1988) 250;
(b) E. Stryjewski, N. Giordano, Adv. Phys. 26 (1997) 487;
(c) H. Aruga Katori, K. Katsumata, Phys. Rev. B 54 (1996) R9620.

[13] (a) Z.-L. Huang, M. Drillon, N. Masciocchi, A. Sironi, J.-T. Zhao, R. Rabu, P. Pannisod, Chem. Mater. 12 (2000) 2805;
(b) P. Rabu, J.M. Rueff, Z.-L. Huang, S. Angelov, J. Souletie, M. Drillon, Polyhedron 20 (2000) 1677;
(c) P. Rabu, Z.-L. Huang, C. Hornick, M. Drillon, Synthetic Met. 122 (2001) 509.

[14] F. Varret, J. Phys. 37 (1976) C6 (colloque C6).

[15] K. Ohta, K. Tanaka, J. Chromatogr. A 804 (1998) 87.

[16] A.L. Spek, Acta Crystallogr. A 46 (1990) C34.

[17] (a) J.B. Goodenough, Magnetism and the Chemical Bond, Wiley, New York, 1963;
(b) J. Kanamori, J. Phys. Chem. Solids 10 (1959) 87;
(c) J. Kanamori, in: G.T. Rado, H. Suhl (Eds.), Magnetism, vol. I (Chapter 4), Academic Press, New York, 1963, p. 127.

[18] H. Kumagai, Y. Oka, K. Inoue, M. Kurmoo, J. Chem. Soc. Dalton Trans. (2002) 3442.